Coherent Control of Internal Conversion in Strong-Field Molecular Ionization

Brian Kaufman,[1] Tamás Rozgonyi,[2,3] Philipp Marquetand,[4,5,6] and Thomas Weinacht[1]
[1]Department of Physics and Astronomy, Stony Brook University, Stony Brook, New York 11794-3800, USA
[2]Wigner Research Centre for Physics, P.O. Box 49, H-1525 Budapest, Hungary
[3]Research Centre for Natural Sciences, Magyar tudósok Körútja. 2, H-1117 Budapest, Hungary
[4]University of Vienna, Faculty of Chemistry, Institute of Theoretical Chemistry, Währinger Straße 17, 1090 Wien, Austria
[5]Vienna Research Platform on Accelerating Photoreaction Discovery, University of Vienna, Währinger Straße 17, 1090 Wien, Austria
[6]University of Vienna, Faculty of Chemistry, Data Science @ Uni Vienna, Währinger Straße 29, 1090 Wien, Austria

(Received 6 April 2020; revised 25 June 2020; accepted 6 July 2020; published 29 July 2020)

We demonstrate coherent control over internal conversion during strong-field molecular ionization with shaped, few-cycle laser pulses. The control is driven by interference in different neutral states, which are coupled via non-Born-Oppenheimer terms in the molecular Hamiltonian. Our measurements highlight the preservation of electronic coherence in nonadiabatic transitions between electronic states.

DOI: 10.1103/PhysRevLett.125.053202

Electronic coherence decays much more rapidly in molecules than atoms as a consequence of averaging over the different rates of phase advance for different internuclear separations associated with nonlocal nuclear wave functions [1–4]. This is particularly dramatic for polyatomic systems that have many degrees of vibrational freedom over which this averaging occurs. Furthermore, if there is nonadiabatic coupling between electronic states, then it is not clear how the phase between states is maintained [3]. Here, we show via interference that the electronic coherence of a wave function in a molecule that undergoes internal conversion via nonadiabatic (non-Born-Oppenheimer) coupling between electronic states is maintained. We show that this coherence can be used to control the population of different electronic states, and measure its decay time [5–10].

Our measurements are of resonance-enhanced strong-field ionization, in which nonadiabatic coupling between neutral states during the ionization dynamics leads to the population of multiple states of the molecular cation [11,12]. By strong-field ionization, we refer to ionization with field strengths where perturbation theory does not provide an accurate description of the light-matter interaction, and dynamic Stark shifts of intermediate states cannot be ignored. By measuring the photoelectrons with velocity map imaging (VMI) [13] and making use of earlier coincidence measurements that relate the photoelectron spectrum to different states of the molecular cation, we are able to measure the phase-dependent ionization yield to different cationic states [14]. Making use of Dyson correlations between neutral and cationic states [15], and earlier work which studied the resonance enhancement of the ionization yield, we are able to relate the phase-dependent ionization yield to interference in nonadiabatically coupled states of the neutral molecule [16,17]. Previous work by other groups has used the phase or delay of a strong-field infrared laser pulse relative to an extreme ultraviolet pulse train to control the total ionization yield of atoms and diatomic molecules [18–22]. Here, we make use of a shaped infrared field and extend the control to the relative yield of different final states of a polyatomic molecular cation.

We use an amplified Ti:sapphire laser system generating 1 mJ transform limited pulses of 30 fs duration, centered at a wavelength of 780 nm, and operating at a 1 kHz repetition frequency. The pulses are spectrally broadened using supercontinuum generation in an argon gas cell producing a slightly blueshifted spectrum (central wavelength of 750 nm), extending from 600–900 nm [23–25] and compressed to a duration just below 10 fs, using a combination of chirped mirrors and an acousto-optic modulator (AOM) based pulse shaper [26,27]. They are characterized using collinear, pulse-shaper-assisted, second harmonic generation frequency resolved optical gating [28,29].

The pulse shaper uses an AOM as a spectral mask $M(\omega)$ to shape the pulse in the frequency domain by placing it in the Fourier plane of a zero dispersion stretcher [30]. The shaped electric field $E'(\omega)$ is a product of the acoustic mask $M(\omega)$ and the unshaped field, $E(\omega)$: $E'(\omega) = M(\omega)E(\omega)$. We used a mask of the form

$$M(\omega) = A\{1 + a\cos[-\tau(\omega - \omega_L) + \phi]\} \qquad (1)$$

to generate a pulse pair with controllable relative pulse amplitude a, time delay τ, laser locking frequency ω_L, relative phase between pulses ϕ, and a controllable overall mask amplitude A. We measured the momentum-resolved photoelectron yield as a function of A, a, τ, ω_L, and ϕ.

As discussed in detail in an earlier publication [31], a unique aspect of the pulse shaper in comparison with an

interferometer is its ability to generate pulse pairs with independent control over the relative amplitude and phase for each delay. This allows us to compensate for delay or phase-dependent intensity variations when the delay between pulses is comparable to the pulse duration. We could therefore adjust the amplitude of the pulses A, in order to maintain a constant peak intensity for different phases, as measured by the phase-dependent second harmonic generation yield and checked by measuring the delay dependent ionization of water [31]. The measurements with and without this intensity compensation are similar and are compared directly in the Supplemental Material [32].

Additionally, the pulse shaper allows us to define a locking frequency ω_L, which is the frequency at which the relative phase between the two pulses is maintained or "locked" (i.e., for which constructive optical interference will occur for all time delays). By default, we chose the locking frequency to correspond to the central wavelength of the pulses, 750 nm. However, we carried out many measurements of the ionization yield as a function of locking frequency. These can be found in the Supplemental Material [32].

The shaped pulses are focused to $\sim 10^{13}$ W/cm^2 into an effusive molecular beam inside a vacuum chamber with a base pressure of 1×10^{-10} torr. The molecules of interest (CH_2IBr, CH_2I_2, and CH_2BrCl) raise the working pressure to about 4×10^{-6} torr. These molecules are ionized, producing a three-dimensional distribution of photoelectrons. The electrons are velocity map imaged to a dual-stack microchannel plate (MCP) and phosphor screen detector using an electrostatic lens. The two-dimensional projection which maps velocity to position is then recorded by a CMOS camera. A fast algorithm is used to identify the coordinates of each electron hit to construct a synthetic VMI image free of background and detector nonuniformities. By inverse-Abel transforming and angularly integrating the image, we can reconstruct the three-dimensional momentum distribution of the outgoing electrons and the photoelectron spectrum. The apparatus is illustrated in the top panel of Fig. 1.

Our main focus is on pump-probe measurements in which we fixed the delay between the pump and probe pulses and varied their relative phase. Using our VMI detector, we measured the photoelectron spectrum of CH_2IBr as a function of the relative phase between pump and probe pulses, as shown in Fig. 2. There are two clear peaks in energy which are maximized at different phases. On the right of Fig. 2 are energy lineouts (yield as a function of energy for a given phase) which highlight the two peaks that we are able to assign to ionic states D_3 (corresponding to electrons with energies from 0–0.35 eV—red curve) and D_1 (corresponding to electrons with energies from 0.40–0.90 eV—cyan curve) based upon earlier ion-electron coincidence measurements [14]. The two-dimensional map clearly shows that the yield varies with phase, and the lineouts at the bottom of Fig. 2 (yield as a function of phase for a given energy) show

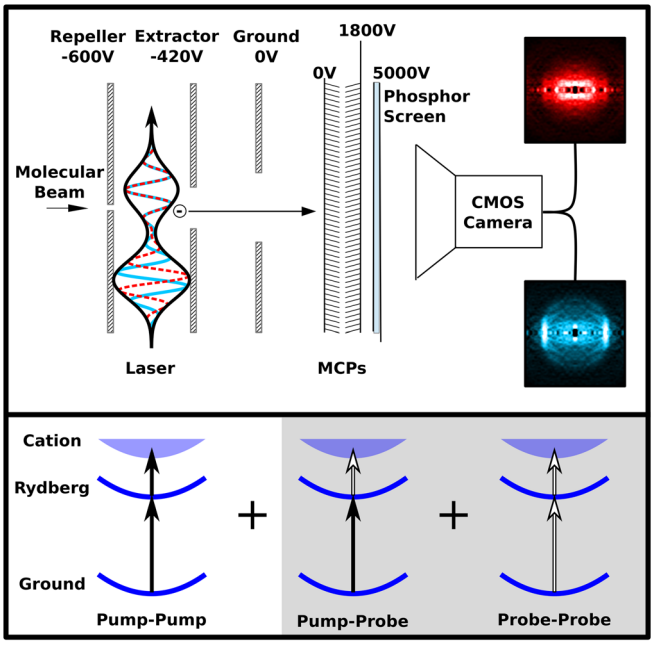

FIG. 1. Top panel: Schematic diagram illustrating the experiment. Two short pulses intersect a molecular beam in a VMI spectrometer. The electrons produced by the laser-molecule interaction are velocity map imaged to the detector and VMI images are recorded for varying phases between pulses. Two Abel-inverted images are shown for the different phases between pulses on the left (blue and red color coding). Bottom panel: Illustration of interfering pathways which lead to phase-dependent ionization yields.

that the two states have a structured phase dependence with their maxima offset by about 1.2π rad.

It is important to confirm, in analyzing the data, that the phase dependence of the yields does not come from optical interference or a phase-dependent variation in the intensity. We note that while the two pulses are separated by more than their durations for the measurements shown in Fig. 2, there is still some overlap and thus variation in the peak intensity with phase. In order to mitigate any modulation in the yields related to these variations in the peak intensity, we performed additional measurements with a phase-dependent amplitude mask, $A(\phi)$, such that the peak intensity is kept constant as the phase is varied. This is accomplished by minimizing the variation in second harmonic yield as a function of phase between the two pulses. The fact that the two states display different offsets in their phase-dependent yield (with or without this amplitude mask, see Supplemental Material [32] for comparison figure) is also consistent with the idea that the phase dependence is driven by molecular interference rather than intensity variations resulting from optical interference.

Having established that the observed interference is not optical, we next turn to the question of whether the interference takes place in neutral states or in the cation.

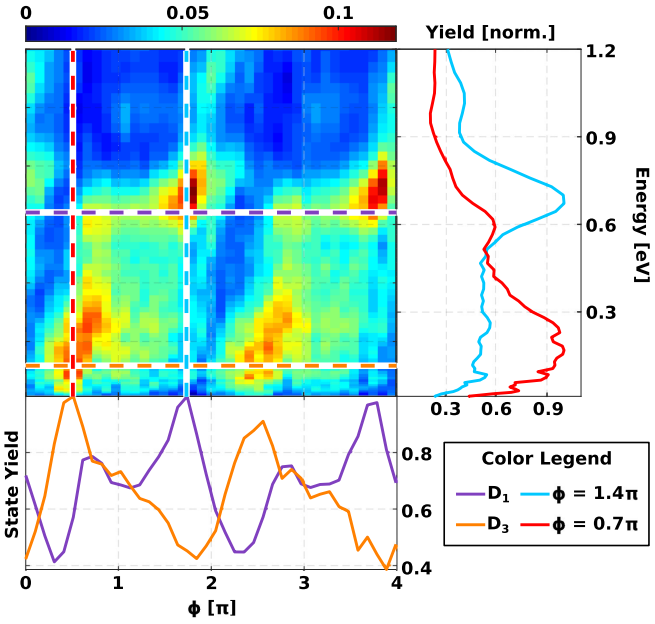

FIG. 2. Main panel: CH_2IBr photoelectron yield as a function of photoelectron energy and phase at a 15 fs delay for pump and probe pulses with fixed energies (i.e., no intensity compensation). Lower panel: Lineouts for the two states of interest D_1 and D_3 as a function of phase, in purple and orange, respectively. Right panel: Lineouts as a function of energy normalized to the total number of detected electrons, i.e., photoelectron spectra for two different phases.

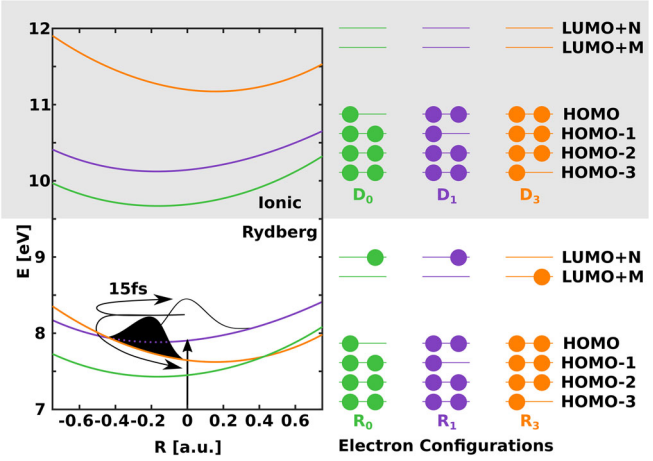

FIG. 3. Potential energy curves and electronic configurations for relevant neutral and ionic states of CH_2IBr. Left panel: potential energy as a function of the CH_2 wagging coordinate for neutral Rydberg states, R_0 (green), R_1 (purple), and R_3 (orange), and ionic states, D_0 (green), D_1 (purple), and D_3 (orange). Cartoon wave packets for the pump (black) and probe (white) are shown for a 15 fs pump-probe delay. Right panel: Electronic configurations for these same states. HOMO corresponds to highest occupied molecular orbital and LUMO corresponds to lowest unoccupied molecular orbital.

If the interference were in the cation, one would expect to see constructive or destructive interference at different electron energies leading to modulations or fringes in the photoelectron spectrum [33]. These fringes would have a period equal to the inverse of the time delay between the pulses, analogous to the fringes seen in an optical spectrometer for two pulses separated by a delay. For a 15 fs delay, one would expect modulations in the photoelectron spectrum with a spacing between peaks or minima of ~0.25 eV. Such modulations are not present in the photoelectron spectrum for 15 fs or any other pump-probe delay.

Further evidence for the interference taking place in the neutral states is provided by the fact that the depth of modulation is more pronounced for an asymmetric pump-probe pulse pair, where the probe pulse is stronger than the pump pulse ($a = 0.7$). This asymmetry supports the idea of interference taking place in the intermediate neutral resonant state because the weak pump predominantly excites the molecules, whereas the stronger probe excites and ionizes, leading to modulations in the ionization yield as a result of interference in the excited state from population transferred by the pump and probe pulses. The cartoon in the lower half of Fig. 1 depicts this by breaking down the ionization yield into three contributing pathways: (1) excitation and ionization by the pump, (2) excitation by the pump and ionization by the probe, (3) excitation and ionization by the probe [34]. The latter two pathways (shaded in the figure) can interfere, leading to phase-dependent ionization yields.

Our understanding of the ionization dynamics in this family of molecules ($CH_2XY, X, Y = Cl, Br, I$) has been developed through multiple experiments and calculations [11,12,35]. These experiments and calculations can be summarized by Fig. 3: intermediate neutral states can be Stark shifted into resonance by the strong-field of the laser pulse, leading to resonance enhancement of multiphoton ionization [36]. This type of resonance during strong-field ionization is known as a "Freeman" resonance [37]. If the pump is short enough (i.e., shorter than the timescale for vibrational dynamics, ~15 fs), then a wave packet launched on the resonant state (because of a nonzero slope at the Franck-Condon (FC) point) does not move much during the pulse, such that the dominant dynamics after excitation are ionization to the cationic state most strongly coupled to the intermediate state. While this simple picture can explain the dominant ionization dynamics for a short pulse, a more complete picture is informed by the fact that the excited neutral states of the molecule are mixed by nonadiabatic coupling near the FC point which can lead to multiple states of the molecular cation [12].

The left hand side of Fig. 3 shows the energies of the relevant neutral and ionic states as a function of the CH_2 wagging coordinate. It is along this coordinate that the relevant states intersect and are coupled via non-Born-Oppenheimer terms in the molecular Hamiltonian. The shaded region of the plot corresponds to ionic states, whereas the unshaded portion corresponds to excited

neutral Rydberg states that are correlated with the ionic states plotted above. The colors indicate which neutral states are correlated with which ionic states. The correlation between the neutral and ionic states is illustrated by the right panel of Fig. 3, which shows the dominant electron configurations for the neutral (Rydberg) and ionic states based on our electronic structure calculations [12]. The configurations of R_0, R_1, and R_3 are nearly identical to those of D_0, D_1, and D_3, respectively. Thus, for these Rydberg states, ionization from R_n to D_m with $n = m$ (n, $m = 0$, 1, 3) is driven by Dyson or Koopmans's correlations [17,38]. Ionization from R_n to D_m with $n = m$ simply involves the removal of a single electron, whereas ionization from R_n to D_m with $n \neq m$ involves the rearrangement of multiple electrons, and is thus suppressed for Rydberg states even in the case of multiphoton coupling [17]. Note that the configuration of R_3 involves a singly occupied LUMO + M orbital, whereas the configurations of R_1 and R_0 involve a LUMO + N. This explains why the neutral states cross, but the ionic states correlated with them (D_0, D_1, and D_3) do not, because the energy required to remove a LUMO + M electron is greater than that required to remove a LUMO + N for $N > M$.

Earlier work established that for a very short pulse (shorter than the vibrational period associated with CH_2 wagging) with a peak intensity $\sim 10^{13}$ W/cm^2, R_1 comes into resonance and enhances the ionization to D_1. However, for longer pulses, there is time for population to spread to R_3 and R_0, leading to multiple states of the cation (D_0 and D_3, in addition to D_1) [12]. The black and white Gaussians on the neutral potentials in the left panel of Fig. 3 illustrate the evolution of wave packets launched by the pump and probe pulses, respectively. Summarizing the resonant enhanced strong-field ionization dynamics, it can be broken down into a three step process: (1) Stark shifting of an intermediate Rydberg state into multiphoton resonance, (2) internal conversion between Rydberg states, and (3) coupling to the continuum (ionization) [31].

As Fig. 3 shows, R_1 and R_3 cross very near the FC point—at a distance comparable to the width of the ground state wave function (the FWHM of the probability distribution is about 0.5 a.u., while the distance between the FC and crossing is about 0.4 a.u.). Thus, it is a mixture of R_1 and R_3 that is excited by the pump pulse. This mixture of neutral states is supported by the photoelectron spectrum for a single short pulse, which exhibits a mixture of ionic states correlated with R_1 and R_3: D_1 and D_3. The mixture is influenced by the duration of the pump pulse, since vibrational dynamics on R_1 near the crossing can cause the wave packet to move to regions of the potential that have more R_3 character. The corresponding ionization leads then to a mixture of D_1 and D_3 that contains more D_3, as we observed in earlier pump-probe measurements [31]. The Supplemental Material [32] illustrates this by showing the photoelectron spectrum for a long and short pulse.

Given the rapid mixing between R_1 and R_3, a probe pulse applied a short time after the pump can excite a second wave packet on R_1 and R_3, which can interfere with the wave packet generated in these states by the pump pulse. The interfering wave packets in these excited states can be ionized by the probe pulse, as illustrated in Fig. 1. The measurements shown in Fig. 2 illustrate the fact that the electronic coherence of the wave functions on R_3 and R_1 is not destroyed by the nonadiabatic coupling, and leads to interference, which in turn leads to phase-dependent variations in the ionization yield to D_3 and D_1 [39].

In order to further test our interpretation of the measurements, we carried out similar measurements on the homologous molecules CH_2I_2 and CH_2BrCl [40]. CH_2I_2 was chosen because, due to symmetry, there is no excitation along the CH_2 wagging mode for intermediate neutral states. Thus, the expectation was that nonadiabatic dynamics should be precluded during the ionization and we should observe no change in the photoelectron spectrum with pulse duration (or delay for two pulses). CH_2BrCl was chosen to check whether we could measure similar phase-dependent yields for a system in which similar dynamics are expected.

As expected, we measured a single peak in the photoelectron spectrum for CH_2I_2 and found no change in the photoelectron spectrum as a function of pulse duration. In contrast, measurements on CH_2BrCl gave very similar results to CH_2IBr, with phase-dependent yields to different ionic states for a pump-probe pulse pair.

In order to compare the measurements on CH_2BrCl and CH_2IBr and see how the coherence varies with pump-probe

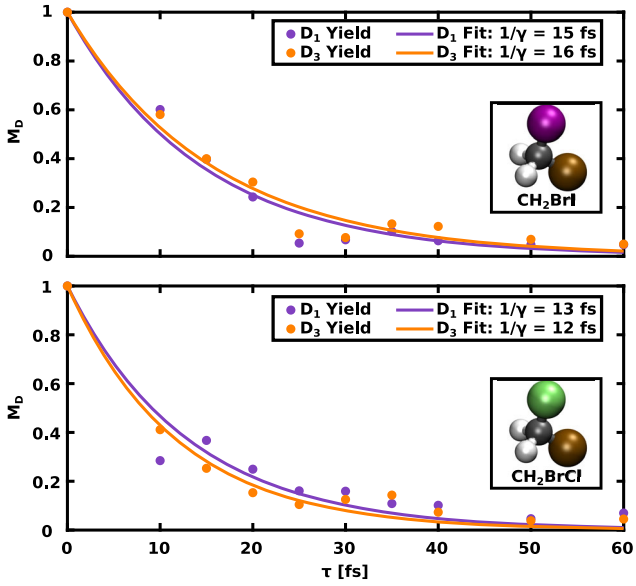

FIG. 4. Depth of modulation (M_D) vs pump probe delay (τ). The top panel shows results for CH_2IBr and the bottom panel for CH_2BrCl. The data points of the M_D were fit to an exponential decay $e^{-\gamma\tau}$. The coherence time is displayed in the legend.

delay, we measured the depth of modulation ($M_D = [\max(Y) - \min(Y)]/[\max(Y) + \min(Y)]$) in the yield Y as a function of phase for different time delays. The results of these measurements are shown in Fig. 4.

For a simple analysis of the data, we fit a decaying exponential to the measurements for each state and find fitted decays or coherence times to be ∼15–16 fs for CH_2IBr, and ∼12–13 fs for CH_2BrCl. This comparison shows that the measurement and the underlying dynamics are not limited to a single molecule, and that while the coherence times for the two molecules are slightly different, they are both on the 10^{-14} s timescale—shorter than the times measured in earlier control experiments that used phase-locked pulse pairs to control the fluorescence of dye molecules on a surface [41], but long enough to dramatically alter the ionization yield via interference between two pulses.

In conclusion, we use shaped, few-cycle laser pulses to demonstrate coherent control over internal conversion during strong-field molecular ionization. Our measurements show that the electronic coherence survives nonadiabatic coupling between states, and we determine the electronic coherence times for two similar molecules.

This work has been supported by National Science Foundation under Grant No. 1806294. It was also partly supported by the Government of Hungary and the European Regional Development Fund under Grant No. VEKOP-2.3.2-16-2017-00015.

[1] B. Gu and I. Franco, J. Phys. Chem. Lett. **9**, 773 (2018).
[2] W. Hu, B. Gu, and I. Franco, J. Chem. Phys. **148**, 134304 (2018).
[3] C. Arnold, O. Vendrell, R. Welsch, and R. Santra, Phys. Rev. Lett. **120**, 123001 (2018).
[4] L. E. Aebersold, I. S. Ulusoy, and A. K. Wilson, Phys. Rev. A **100**, 023406 (2019).
[5] M. Wollenhaupt, T. Bayer, and T. Baumert, in *Ultrafast Dynamics Driven by Intense Light Pulses* (Springer, Cham, 2016), pp. 63–122.
[6] Y. Silberberg, Annu. Rev. Phys. Chem. **60**, 277 (2009).
[7] I. R. Sola, J. González-Vázquez, R. de Nalda, and L. Banares, Phys. Chem. Chem. Phys. **17**, 13183 (2015).
[8] R. J. Gordon and S. A. Rice, Annu. Rev. Phys. Chem. **48**, 601 (1997).
[9] M. Shapiro and P. Brumer, *Quantum Control of Molecular Processes* (John Wiley & Sons, Weinheim, 2012).
[10] E. Wells, C. Rallis, M. Zohrabi, R. Siemering, B. Jochim, P. Andrews, U. Ablikim, B. Gaire, S. De, K. Carnes *et al.*, Nat. Commun. **4**, 2895 (2013).
[11] V. Tagliamonti, P. Sándor, A. Zhao, T. Rozgonyi, P. Marquetand, and T. Weinacht, Phys. Rev. A **93**, 051401 (R) (2016).
[12] P. Sándor, V. Tagliamonti, A. Zhao, T. Rozgonyi, M. Ruckenbauer, P. Marquetand, and T. Weinacht, Phys. Rev. Lett. **116**, 063002 (2016).
[13] A. T. J. B. Eppink and D. H. Parker, Rev. Sci. Instrum. **68**, 3477 (1997).
[14] P. Sándor, A. Zhao, T. Rozgonyi, and T. Weinacht, J. Phys. B **47**, 124021 (2014).
[15] C. Melania Oana and A. I. Krylov, J. Chem. Phys. **127**, 234106 (2007).
[16] M. Spanner, S. Patchkovskii, C. Zhou, S. Matsika, M. Kotur, and T. C. Weinacht, Phys. Rev. A **86**, 053406 (2012).
[17] W. D. M. Lunden, D. Geißler, P. Sándor, T. C. Weinacht, and T. Rozgonyi, Phys. Rev. A **89**, 053404 (2014).
[18] P. Johnsson, J. Mauritsson, T. Remetter, A. L'Huillier, and K. J. Schafer, Phys. Rev. Lett. **99**, 233001 (2007).
[19] W. Siu, F. Kelkensberg, G. Gademann, A. Rouzée, P. Johnsson, D. Dowek, M. Lucchini, F. Calegari, U. De Giovannini, A. Rubio *et al.*, Phys. Rev. A **84**, 063412 (2011).
[20] P. Ranitovic, X. M. Tong, C. W. Hogle, X. Zhou, Y. Liu, N. Toshima, M. M. Murnane, and H. C. Kapteyn, Phys. Rev. Lett. **106**, 193008 (2011).
[21] N. Shivaram, H. Timmers, X.-M. Tong, and A. Sandhu, Phys. Rev. Lett. **108**, 193002 (2012).
[22] P. Ranitovic, C. W. Hogle, P. Rivière, A. Palacios, X.-M. Tong, N. Toshima, A. González-Castrillo, L. Martin, F. Martín, M. M. Murnane *et al.*, Proc. Natl. Acad. Sci. U.S.A. **111**, 912 (2014).
[23] L. Gallmann, T. Pfeifer, P. M. Nagel, M. J. Abel, D. M. Neumark, and S. R. Leone, Appl. Phys. B **86**, 561 (2007).
[24] C. P. Hauri, W. Kornelis, F. W. Helbing, A. Heinrich, A. Couairon, A. Mysyrowicz, J. Biegert, and U. Keller, Appl. Phys. B **79**, 673 (2004).
[25] F. Hagemann, O. Gause, L. Wöste, and T. Siebert, Opt. Express **21**, 5536 (2013).
[26] G. Stibenz, N. Zhavoronkov, and G. Steinmeyer, Opt. Lett. **31**, 274 (2006).
[27] M. A. Dugan, J. X. Tull, and W. S. Warren, J. Opt. Soc. Am. B **14**, 2348 (1997).
[28] R. Trebino, K. W. DeLong, D. N. Fittinghoff, J. N. Sweetser, M. A. Krumbügel, B. A. Richman, and D. J. Kane, Rev. Sci. Instrum. **68**, 3277 (1997).
[29] I. Amat-Roldán, I. G. Cormack, P. Loza-Alvarez, E. J. Gualda, and D. Artigas, Opt. Express **12**, 1169 (2004).
[30] A. M. Weiner, Rev. Sci. Instrum. **71**, 1929 (2000).
[31] V. Tagliamonti, B. Kaufman, A. Zhao, T. Rozgonyi, P. Marquetand, and T. Weinacht, Phys. Rev. A **96**, 021401(R) (2017).
[32] See Supplemental Material at http://link.aps.org/supplemental/10.1103/PhysRevLett.125.053202 for photoelectron spectra for different pulse durations, phase scans with and without intensity compensation, and scans of the phase-locking frequency.
[33] M. Wollenhaupt, A. Assion, D. Liese, C. Sarpe-Tudoran, T. Baumert, S. Zamith, M. A. Bouchene, B. Girard, A. Flettner, U. Weichmann *et al.*, Phys. Rev. Lett. **89**, 173001 (2002).
[34] R. Jones, Phys. Rev. Lett. **75**, 1491 (1995).
[35] D. Geißler, T. Rozgonyi, J. González-Vázquez, L. González, P. Marquetand, and T. C. Weinacht, Phys. Rev. A **84**, 053422 (2011).
[36] G. N. Gibson, R. R. Freeman, and T. J. McIlrath, Phys. Rev. Lett. **67**, 1230 (1991).

[37] R. R. Freeman and P. H. Bucksbaum, J. Phys. B **24**, 325 (1991).
[38] T. Koopmans, Physica (Utrecht) **1**, 104 (1934).
[39] The strong fields involved in the experiment preclude the use of an N photon perturbative description, for which one would expect N modulations in the yield per 2π phase. Thus, there is a more complicated phase dependence, with modulations (Fourier components) in the yield at multiple frequencies. Averaging over the different intensities in the focal volume of the laser leads to a damping of the higher frequency modulations, emphasizing the lower frequency modulations (one and two modulations per 2π phase), which dominate our measurements.
[40] K. M. Tibbetts, X. Xing, and H. Rabitz, Phys. Chem. Chem. Phys. **15**, 18012 (2013).
[41] R. Hildner, D. Brinks, and N. F. Van Hulst, Nat. Phys. **7**, 172 (2011).